Dark-field light scattering imaging of living cancer cell component from birth through division using bioconjugated gold nanoprobes

Wei Qian
Georgia Institute of Technology
School of Chemistry and Biochemistry
Laser Dynamics Laboratory
901 Atlantic Drive
Atlanta, Georgia 30332

Xiaohua Huang
Georgia Institute of Technology
School of Chemistry and Biochemistry
Laser Dynamics Laboratory
901 Atlantic Drive
Atlanta, Georgia 30332
and
Emory University and Georgia Institute of Technology
Emory-Georgia Tech Cancer Center for Nanotechnology Excellence
Department of Biomedical Engineering
Clinic B Room B3211
1365-B Clifton Road Northeast
Atlanta, Georgia 30322

Bin Kang
Mostafa A. El-Sayed
Georgia Institute of Technology
School of Chemistry and Biochemistry
Laser Dynamics Laboratory
901 Atlantic Drive
Atlanta, Georgia 30332

Abstract. Novel methods and technologies that could extend and complement the capabilities of the prevailing fluorescence microscope in following the cell cycle under different perturbations are highly desirable in the area of biological and biomedical imaging. We report a newly designed instrument for long-term light scattering live cell imaging based on integrating a homebuilt environmental cell incubation minichamber and an angled dark-field illumination system into a conventional inverted light microscope. Peptide-conjugated gold nanoparticles that are selectively delivered to either the cytoplasmic or nuclear region of the cell are used as light scattering contrast agents. The new system enables us to carry out continuous and intermittence-free dark-field live cell imaging over several tens of hours. A variety of applications of this imaging system are demonstrated, such as monitoring the nuclear uptake of peptide-conjugated gold nanoparticles, tracking the full cycle of cancer cells from birth to division, following the chromosome dynamics during cell mitosis, and observing the intracellular distribution of gold nanoparticles after cell division. We also discuss the overall effect of nuclear targeting gold nanoparticles on the cell viability of parent and daughter cells. [DOI: 10.1117/1.3477179]

Keywords: light scattering imaging; dark field; real time; gold nanoparticles; nuclear targeting; mitosis; cell cycle.

Paper 09489RR received Nov. 9, 2009; revised manuscript received May 19, 2010; accepted for publication Jun. 25, 2010; published online Aug. 13, 2010.

1 Introduction

Optical imaging has been widely used in biology and medicine for noninvasive visualization of cellular and molecular features and processes *in vitro* and *in vivo*.[1–7] One of the classic optical techniques is fluorescence imaging, which has the capability of tracking individually labeled molecules with high spatial and temporal resolution.[8–13] It has thus played important roles in interrogating many biological processes such as the mitotic dynamics of chromosomes, centrosomes, and spindles;[14–17] protein folding and migration of membrane proteins;[18–20] cell signaling;[10] and virus trafficking.[21,22] Multiplex imaging can be performed by using fluorescent probes with different emission wavelengths. However, fluorescence has intrinsic disadvantages of photobleaching and blinking,[23–28] so it is not useful for long-term (several tens of minutes to hours) imaging studies. To image cellular processes over a long period of time without phototoxicity, light scattering imaging based on the detection of elastic scattered light from investigated species has become a very promising option. The use of light scattering contrast agents not only enables investigation of cellular structures or processes of specific interest, but also significantly enhances the imaging sensitivity.

The strongly enhanced light scattering property of gold nanoparticles (Au NPs) owing to the localized surface plasmon resonance, together with their excellent photostability and biocompatibility, makes them powerful contrast agents in light scattering imaging.[29,30] Using an angled dark-field illuminator coupled with a conventional microscope, Yguerabide et al. demonstrated that resonance light scattering Au NPs can be used as ultrasensitive labels for analyte detection in immuoassays, cells, and tissues.[31] The studies by Sokolov et al. show that Au-NP-labeled cervical cancer cells and tissues can be well resolved from normal ones on illumination with single wavelength laser light either from a simple laser pen or the excitation laser light from a confocal microscope.[32] Later, true-color Au-NP-enhanced cancer cell imaging was achieved with commercial dark-field microscopy.[33] Because of the advantages of simplicity, low cost, and availability, this resonance light scattering imaging of Au NPs with commercial dark-field microscopy has gained intense attention in biological and biomedical research.[34–37] Recently, several groups have applied this technology to monitor the dynamic interac-

Address all correspondence to: Mostafa A. El-Sayed, 901 Atlantic Drive, Atlanta, Georgia 30332. Tel: 404-894-0292; Fax: 404-894-0294. E-mail: melsayed@gatech.edu

1083-3668/2010/15(4)/046025/9/$25.00 © 2010 SPIE

tions between biomolecules in live cells in real time.[38–41] In their studies, commercially available flow chambers containing cells and culture media were used for live cell imaging. The flow chambers were placed into the narrow space between an oil-immersion dark-field condenser with a high numerical aperture (NA) and the high-magnification objective. Although live cell imaging could be recorded, the shortcomings of this setup were apparent. First, the cells in the flow chamber are exposed to nonuniform shear stress due to fluid flows. Shear stress affects physiological and biochemical processes in the cells. Thus, the cells under investigation are no longer the same as the original cells. This could render experimental artifacts. Second, the regular flow chambers require a large cell culture volume and thus massive amounts of Au NP bioconjugates.

In this paper, we report a newly designed instrumental system that provides the ability of light scattering imaging of live cells for two full cell cycles. By combining a conventional inverted microscope, an angled white light illuminator, and a homebuilt environmental cell incubation minichamber, the new instrument enables us to carry out continuous, intermittence-free and long-term (as long as 30 h) dark-field live cell imaging enhanced by resonant light scattering Au NPs. We also show several applications of this real-time imaging system including monitoring the nuclear uptake of bioconjugated Au NPs, tracking the full cycle of cancer cells from birth to division, following the nuclear dynamics during cell mitosis, observing the intracellular distribution of Au NPs, and visualizing the effect of Au NPs on cell viability. Cancer cells were selected for this study not only because we could selectively deliver Au NPs into the cell nuclear region using RGD (arginine-glycine-aspartic acid) and nuclear location sequence (NLS) peptides or the cytoplasm region using RGD alone, but also because of the importance of cancer research, as cancer remains as one of the leading causes of death in the United States and many other parts of the world.

2 Materials and Methods

2.1 *Synthesis and Peptide Conjugation of Au NPs*

Au NPs were synthesized according to the well-established citrate-reduction method.[42,43] Briefly, 50 mL of a 0.01% (by weight) auric acid (Sigma-Aldrich) aqueous solution was heated to boiling while stirring in a 100-mL beaker. Next, 350 μL of a 1% (by weight) trisodium citrate (Sigma-Aldrich) aqueous solution was quickly added. The solution changed color within several minutes from yellow to black and then to red, indicating NP formation. The absorption spectrum of the NPs measured by a UV-Vis spectrometer (Ocean Optics) shows the surface plasmon resonance wavelength at around 526 nm. Transmission electron microscopy (TEM, JEOL 100CX II) and dynamic light scattering (DLS, ZetaSizer Nano ZS90) show the size of the NPs at about 30 nm in diameter.

Before peptide conjugation, Au NPs were modified with thiolated poly(ethylene) glycol (PEG). This was done by mixing 0.8 nM citrate capped Au NPs (calculated concentration using $\varepsilon_{abs}=3.0\times10^9$ M^{-1} cm^{-1} determined by Hurst et al.[44]) with 2 μM methoxy-PEG-thiol (mPEG-SH, molecular weight 5000, Laysan Bio, Inc.) for 2 h at room temperature. The PEGylated Au NPs were centrifuged at 14,000 rpm for 20 min and redispersed in PBS (phosphate-buffered saline) buffer to a final optical density of 2.0. The NLS (CGGGPKKKRKVGG), originating from the SV-40 large T antigen[45–47] and $\alpha_v\beta_3$ integrin targeting arginine-glycine-aspartate containing peptide (RGDRGDRGDRGDPGC) were bound to Au NPs via Au-S bonds at the cysteine residues. This was done by mixing 50 μM RGD alone (for cytoplasmic delivery) or both 50 μM RGD and 50 μM NLS (for nuclear delivery) with 1 nM PEGylated Au NPs. The mixtures were allowed to react overnight. The peptide-conjugated Au NPs were purified by centrifugation at 14,000 rpm for 20 min and then redispersed in PBS buffer. The surface modification at each step was monitored by changes in the absorption spectra, size, and zeta potential.

2.2 *Cell Culture and Au NP treatment*

Human oral squamous cell carcinoma (HSC-3) cells were cultured in Dulbecco's modification of Eagle's medium (DMEM, Cellgro) plus 10% fetal bovine serum (FBS, Gem Cell) at 37 °C under 5% CO_2. The cells were first placed in a 35-mm glass-bottomed tissue culture dish and allowed to grow for 2 days. Then a given volume of Au NPs with an optical density of 2.0 was added to the medium to a final concentration of 0.05 to 0.4 nM. The cells were incubated with the NP-containing medium for 24 h. Then, the cells were washed with 1× PBS, immersed in fresh medium, and put in the cell incubation minichamber on the microscope for real-time dark-field live cell imaging. For the particle-tracking experiments, the cell dish was put into the minichamber for imaging immediately after Au NP addition.

2.3 *Real-Time Dark-Field Light Scattering Imaging*

Figure 1(a) shows the instrumental setup of the real-time dark-field light scattering imaging system. This system is a combination of a commercial inverted Olympus IX70 microscope, an angled white light illumination system, and a homebuilt environmental cell culture minichamber. In the conventional dark-field microscope, a high-NA condenser is used to deliver a narrow beam of white light onto the top of the sample. In our study, the dark-field illumination system was angled with respect to the sample plane, similar to the setup described by Yguerabide et al.[30] This side-illumination arrangement enabled for the location of a homebuilt environmental cell culture minichamber on the microscope stage. The side illumination system was composed of a Fiber-Lite MI-150 white light illuminator (Dolan-Jenner Industries), an optical fiber delivering the light closer to the sample, and a condenser lens focusing the light onto the sample. Using a sample of dried Au NPs on a microscope cover glass, the illumination angle and the focus were optimized so that there was no uneven illumination and the transmission light did not enter the objective (40× iris, U Plan FL, NA 0.6, WD2.7). At the sample position, the light beam was about 2 mm in diameter.

The environmental chamber, which was made of a double wall of organic glass and a copper bottom with a hole in the middle for light transmission, was connected with a heated/refrigerated circulator (VWR) and with a gas tank containing 5% CO_2 in air. A temperature of 57 °C of the water in the circulator tank gave a temperature of 37 °C of the medium in

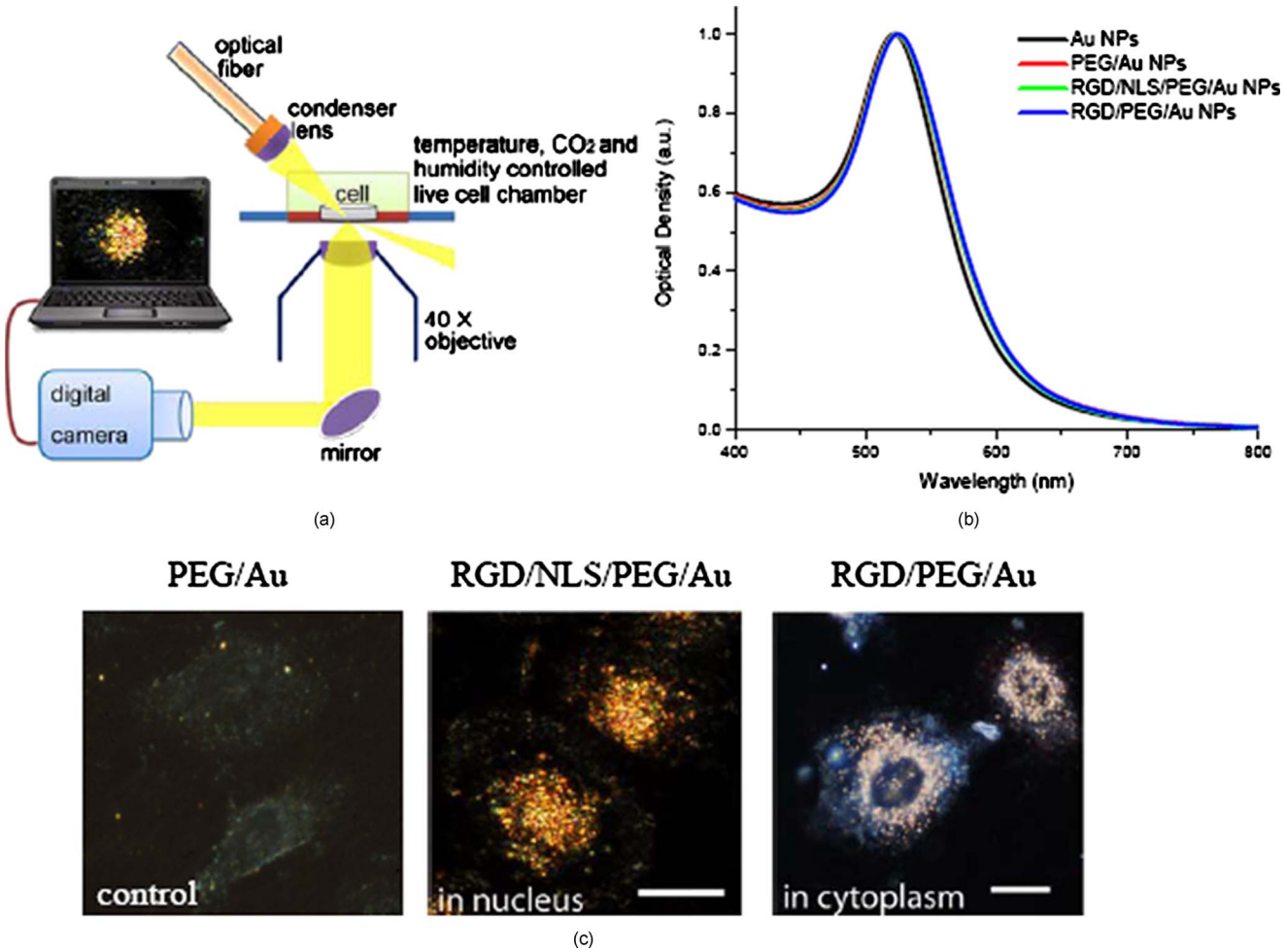

Fig. 1 Imaging setup and particle targeting strategy. (a) Schematic setup of real-time light scattering imaging system for live cell studies. A dark-field light scattering imaging microscope with a side-illumination arrangement is combined with a homebuilt environmental cell incubation chamber for long-time study of live cells. (b) Absorption spectra of Au NPs before and after surface modification. Surface modification with mPEG-SH molecules induces an ~3-nm red shift of the localized surface plasmon resonance wavelength of the Au NPs. Additional binding of RGD/NLS or RGD leads to a further 2- to 3-nm red shift of the plasmon wavelength maximum of the nanoparticles. (c) Typical images of HSC-3 cancer cells after incubation with 0.1 nM PEG conjugated (left), RGD/NLS/PEG conjugated (middle) and RGD/PEG conjugated (right) Au NPs for overnight in cell culture medium at 37 °C. While the PEG conjugated Au NPs do not bind to the cells, RGD/NLS/PEG conjugated ones were accumulated in cell nuclear region and the RGD/PEG conjugated ones were accumulated in cytoplasm. Scale bar: 10 μm. (Color online only.)

the cell culture dish in the chamber. The opened water channel in the wall of the chamber served as a humidity reservoir as well to prevent culture from desiccation (humidity: >95%). The CO_2 flow rate was monitored by a solid acrylic flow meter (Davis Instruments) and adjusted to around 2 scfh (standard cubic feet per hour) to maintain cell culture medium pH. This environmental cell culture system enabled live cell studies in real time over 30 h. The images were taken using a Nikon D200 digital camera. A blank microscope cover glass was used to perform a manual white balance of the camera.

3 Results and Discussion

3.1 *Monitoring Nuclear Uptake of Peptide-Conjugated Au NPs*

Nuclear targeting of NPs is a topic of great importance not only for understanding fundamental gene functions but also for developing gene delivery technology. Nuclear delivery is largely dependent on the use of nuclear localization signals, amino acid sequences that viruses generally use for nuclear entry via interaction with the nuclear pore complex.[48,49] The nuclear localization of Au NPs modified with an NLS peptide from the SV-large T antigen was reported by Xie et al. using TEM and surface-enhanced Raman spectroscopy[50] and by Ryan et al. using inductively coupled plasma optical emission spectroscopy (ICP-OES) and nuclear fractionation techniques.[51] In our previous study, we observed the nuclear localization of NLS-conjugated Au nanorods using a dark-field microscope and confirmed it with surface-enhanced Raman spectroscopy.[47] In this work, we modified NLS-conjugated Au NPs by adding a linear RGD peptide to facilitate nuclear targeting of cancer cells, taking advantage of the specific binding of RGD peptides to $\alpha_v\beta_3$ integin receptors overexpressed on many types of cancer cells and tumor vasculature.[52–54] To overcome NP aggregation by the peptide molecules, we stabilized the NPs with a minimal amount of

Table 1 Physicochemical properties of plain and surface modified Au NPs with PEG, NLS/RGD/PEG, and RGD/PEG molecules.

	Au NP	PEG/Au	RGD/NLS/PEG/Au	RGD/PEG/Au
Hydrodynamic size (nm)	30±1	41±2	46±2	46±2
Zeta potential (mV)	−40±3	−10±2	−4±2	−15±2

PEG in advance. Subsequent addition of both RGD and NLS produces Au NPs capped with a mixed monolayer of RGD, NLS, and PEG molecules. Surface modification with mPEG-SH molecules induces about a 3-nm red shift of the NP-localized surface plasmon resonance wavelength [Fig. 1(b)] and a 10-nm increase on the hydrodynamic diameter. The zeta potential dramatically dropped from −40 to −10 mV after PEGylation (Table 1). Additional binding of RGD/NLS leads to a further 2 to 3-nm plasmon wavelength shift and a 5-nm hydrodynamic size change due to the conformational change of PEG molecules after adding peptides. Comparatively, for cytoplasmic NP delivery, the NPs were conjugated with PEG and RGD only. Surface characterization with an absorption spectrum and DLS shows similar changes for dual functionalization. The difference in zeta potential is due to the positive charge contributed by the NLS peptides. Figure 1(c) shows that PEG-conjugated Au NPs do not bind to the HSC-3 cancer cells. The RGD/PEG-conjugated Au NPs were found in the cytoplasm only. The addition of the NLS peptide leads to a predominantly nuclear accumulation of NPs. Our recent study[55] shows that the NLS/RGD/PEG-conjugated Au NPs, at a high concentration, cause DNA damage in cancer cells, but the RGD/PEG-conjugated Au NPs do not. This confirms the success of nuclear targeting by the dual functional Au NPs.

Using the real-time light scattering imaging system, we could continuously observe, over hours, how the NPs enter into cells and how they accumulate in the nuclear region. The transport of NLS/RGD/PEG-conjugated Au NPs into single cells within 15 h is shown in Fig. 2. Consecutive dark-field light scattering images show the full process of the nuclear localization of NPs in the presence of 0.05 nM NLS/RGD/PEG-conjugated Au NPs [Fig. 2(a)], which shows that NPs are found in nuclear region within 3 h. Massive nuclear accumulation takes about 13 h, which is consistent with results reported by the literature using a commercial incubator.[50] This confirms that our homebuilt minichamber used for imaging live cells does provide a growth environment very similar to that offered by the commercial incubator.

The observed nuclear localization indicates that the NPs do escape from the endosome by a yet unknown mechanism and are able to gain access to the nucleus. From Fig. 2(a), we can see that the Au NPs are first distributed in the cytoplasm (1-h image). Then Au NPs penetrate the nuclear membrane and accumulate in the nucleus over time. Finally, the NPs were found to be localized predominately inside the nuclear region after 7 h (Video 1). The nuclear internalization is possibly via the following steps. First, the NPs must enter into the cytoplasm, most probably by receptor-mediated endocytosis because the RGD on the NPs binds to the integrin receptors on the cancer cell surface. Then the NPs escape from the endosome and transport to the nuclear region. Finally, the NPs transpass nuclear membrane and are accumulated in the nuclear region. There is an alternative way for the RGD/NLS/PEG-conjugated Au NPs to accumulate in the nuclear region after long-term internalization. First, the NPs enter into the cell via the endocytic pathway, probably via receptor-mediated endocytosis. Second, the NPs move toward the Golgi apparatus and endoplasmic reticulum (ER) via retrograde transport and late endosomes to the Golgi apparatus pathway. Third, once at the ER via retrograde transport, the NPs have access to the nucleus envelope and finally to the nuclear region.

It is possible that the Au NPs inside the nuclear region bind to macromolecules, such as DNA, RNA, or proteins. As a matter of fact, molecular signatures from DNA and proteins in

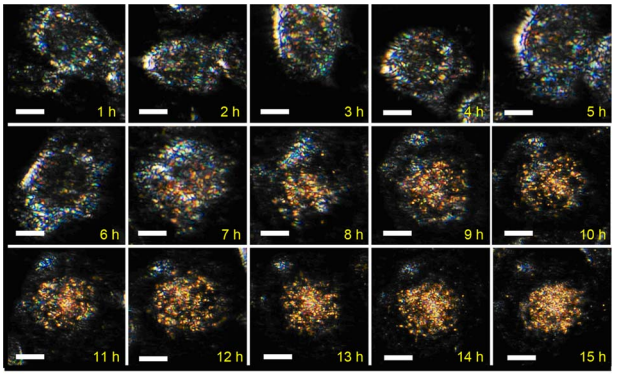

(a)

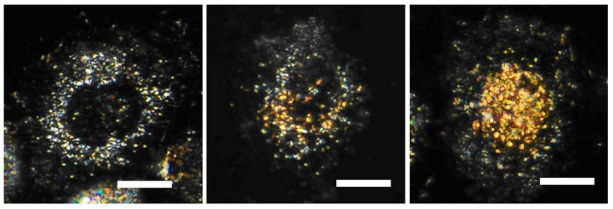

(b)

Fig. 2 Real-time tracking of the nuclear uptake of RGD- and NLS-conjugated Au NPs in HSC-3 cancer cells. (a) Time-dependent nuclear uptake of RGD/NLS/PEG-conjugated Au NPs (also see supplementary information in Video 1). (b) Changes of color of Au NPs in the three representative stages of nuclear localization, the color of the Au NPs changes from cyan at low density to yellow at higher density after they transport from the cytoplasm (left) to a smaller volume nucleus (right). For both (a) and (b), the cells were immersed in cell culture medium at 37 °C overnight in the presence of 0.05-nM RGD/NLS/PEG-conjugated Au NPs. Scale bar: 10 μm. (Color online only.)

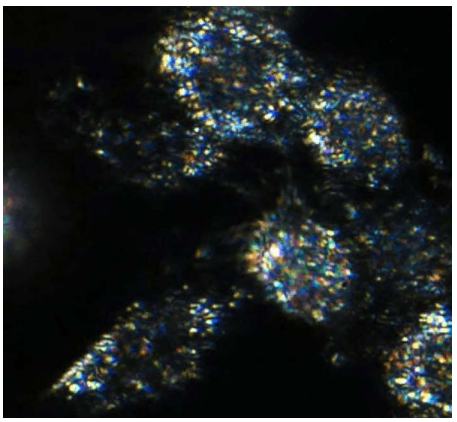

Video 1 Real-time observation of nucleus internalization of NLS Au NPs into cancer cell nucleus (QuickTime, 6 MB).
[URL: http://dx.doi.org/10.1117/1.3477179.1]

the nucleus were reported by our group[47] and other researchers[50] using Raman spectroscopy enhanced by the nuclear targeting Au NPs. Note that although we show here a 15-h tracking experiment, this imaging technique can be used for real-time studies up to at least 30 h. This gives us the opportunities to study the full cycle of a single live cell, as well as the division of second-generation cells as shown in the following section.

Another interesting finding is the change in the color of Au NPs during the process of nuclear internalization. As shown in Fig. 2(b), the image on the left shows Au NPs in the cytoplasm. The image in the middle shows that some NPs penetrate the nuclear membrane and accumulate inside the nuclear region. The image on the right shows the majority of NPs initially in the cytoplasm is now localized in the nucleus. From these results, it can be seen that the color of the Au NPs change from cyan to yellow after transport from the cytoplasm to the nucleus. The red shift of the light scattering wavelength is attributed to the NP plasmonic coupling.[56–58] As the plasmonic fields overlap on aggregation, the color shifts from blue to red.

Using the dark-field imaging system, we demonstrated that the behavior of light scattering Au NPs in living cells as well as that of the cells themselves can be monitored in real time over a long-time duration. However, like all other technologies, our current imaging system has some disadvantages. One of these disadvantages is the uneven illumination. Traditional dark-field microscopy setups are designed to provide even illumination from all sides. In our case, the cells were illuminated from one side. This uneven illumination could induce color artifacts in the images, as indicated by the blue shadows in Fig. 2(a). To eliminate such effects to a large extent, dried Au NPs on a microscope cover glass was used as a standard sample to optimize the illumination angle and the focus. The focus was made as sharp as possible and the transmission light does not enter the objective. In addition to the uneven illumination, there are other limitations, such as low spatial resolution in the direction perpendicular to the image plane and inability to performing multiplex imaging. Therefore, intensive research efforts are still required in the future to address these limitations.

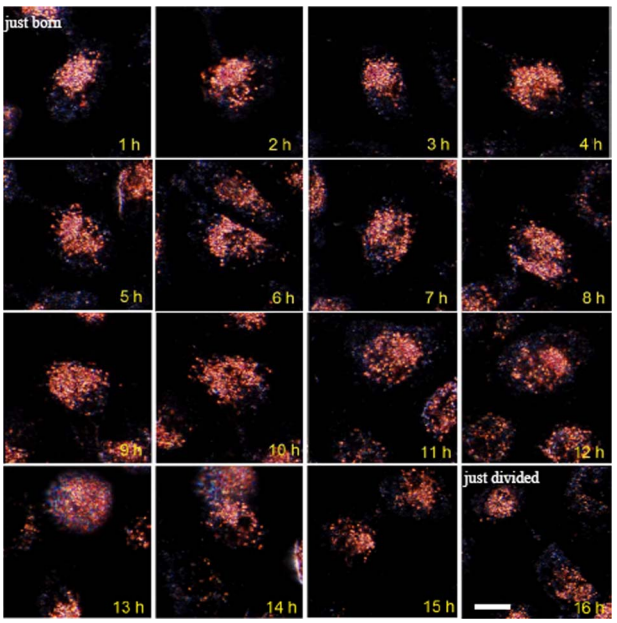

Fig. 3 Real-time tracking of a full cycle of a HSC-3 cancer cell with Au NPs localized in the nuclear region from birth to division. The cells were incubated with 0.1 nM RGD/NLS/PEG-conjugated Au NPs in cell culture medium at 37 °C overnight before the tracking experiment. Using the enhanced real-time light scattering imaging technique, we were able to track the full cycle of a cell from birth to division and monitor the distribution of the nanoparticles in single cells in real time. Labels on the images indicate the time lapse. Scale bar: 10 μm.

3.2 *Tracking the Full Cycle of Cancer Cells from Birth to Division*

Knowledge about the complex processes of the cell cycle is indispensable in understanding cancer formation and progression, and the signaling pathways responsible for human tumorigenesis. It is undoubted that the most straightforward method to investigate the cell cycle is imaging. For mammalian cells, it is a great challenge because of the very long period of the cell cycle (about 24 h) and we could not rely on fluorescence microscopy. Our technique of real-time light scattering imaging enables continuous, intermittence-free, and long-time imaging, providing an approach for dealing with this challenge. Figure 3 shows that consecutive dark-field light scattering images of a living cancer cell in a full cycle from birth to division. Although the G1, S, and G2 phases cannot be clearly resolved, the M phase can be seen occurring between 13 and 15 h. The morphological changes of the cell at these phases can also be observed in real time. While the whole cycle takes as long as over 16 h, the division takes only about 2 h. Note that the NPs remain in the nuclear region after division. This demonstrates that the instrument developed here is capable of real-time cell cycle studies at the single-cell level. This is helpful for investigating the dynamics of a single cell at different phases in a cell cycle.

3.3 *Following Nuclear Dynamics during Cell Mitosis*

Using the imaging technique and Au NPs as contrast agents, we followed especially the mitosis process at a higher time resolution (Fig. 4). The mitosis of eukaryotic cells is a com-

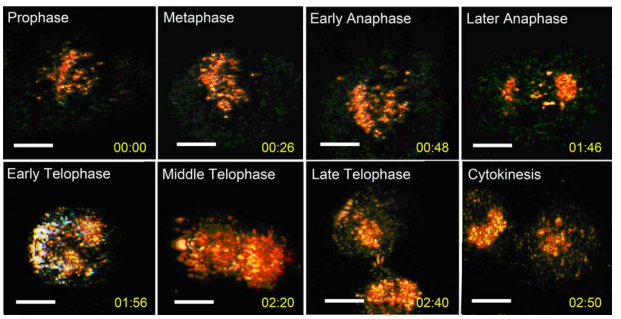

Fig. 4 Real-time tracking of the mitosis process of a HSC-3 cancer cell with Au NPs localized in the nuclear region. The motion of the chromosome at different stage of mitosis is resolved by the light scattering imaging of RGD/NLS/PEG-conjugated Au NPs in the nuclear region (also see supplementary information in Video 2). The cells were incubated with 0.1 nM RGD/NLS/PEG-conjugated Au NPs in a cell culture medium at 37 °C overnight before the tracking experiment. The time lapse shown in each image is as hour:minute. Scale bar: 10 μm.

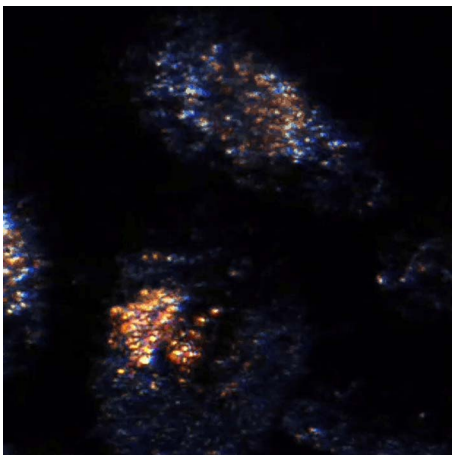

Video 2 Following the nuclear dynamics using Au NPs during cell mitosis (QuickTime, 5 MB).
[URL: http://dx.doi.org/10.1117/1.3477179.2]

plex process involving chromosome condensation, nuclear envelope and lamina disassembly, spindle formation, and movement of varied nuclear proteins.[59–61] Although fluorescence live-cell imaging techniques facilitate the detection of chromosomes and various cellular proteins, the study of dynamical properties of centrosomes and kinetochores, and gain us insights on the molecular mechanisms of tubulin,[14–17] the disadvantages of photobleaching and phototoxicity limit the applications in long-term imaging. The light scattering imaging technique assisted by Au NP contrast agents could be a potential alternative for imaging the complicated process of mitosis in real time. As shown in Fig. 4, subphases from prophase to cytokinesis during the course of mitosis can be well resolved by the light scattering Au NP contrast agents.

Binding of NLS-conjugated Au NPs to chromosomes were previously confirmed by the detection of surface enhanced Raman signals from DNA in single cells,[47,50] so it is not surprising that the RGD/NLS/PEG-modified Au NPs in our study might bind to the chromosomes and enable us to track the chromosome dynamics. It is well known that the configuration of the chromosome keeps changing during mitosis, and the characteristic chromosome pattern is used to identify the different stages of mitosis. From Fig. 4, it is obvious that the evolution of the pattern of Au NP distribution inside of the nucleus exactly follows that of the chromosomes, indicating the binding of Au NPs to the chromosomes. In agreement with results in Fig. 3, it is found that Au NPs, initially inside the nucleus of the parent cell, remain in the nucleus of the daughter cells. Another interesting phenomenon is that Au NPs do not seem to divide equally between the two daughter cells (see Video 2). The capability of resolving every stage of the mitosis process at a single-cell level based on light scattering from peptide-conjugated Au NPs implicates that this new technology has great potential to provide us with new insights in understanding mitosis, a very important cellular process.

3.4 *Observing Intracellular Distribution of Au NPs during Cell Division*

To futher understand the behavior of Au NPs during cell mitosis, we tracked the distribution of Au NPs before and after cell division. By selectively conjugating Au NPs with specific molecules (NLS/RGD or RGD alone), we were able to deliver them either into the nucleus or into the cytoplasm. It is obvious that the final distribution of the Au NPs in daughter cells depends on their initial location in the parent cell (Fig. 5). Both NLS- and RGD-conjugated Au NPs, initially localized in the nucleus of the mother cell, are found in the nucleus of the daughter cells after division (see Video 3). This is consistent with the images shown in the Figs. 3 and 4. RGD-conjugated Au NPs initially localized in the cytoplasm of the mother cell, are found only in the cytoplasm of the daughter cells (see Video 4). It is well known that in mitosis, the nuclear envelope disintegrates during prophase and reforms in telophase. This implies that during the period of metaphase and anaphase, the environment of the nucleus and the cytoplasm completely mix with one another. However, Au NPs remain either in the nuclear or cytoplasmic regions after cell

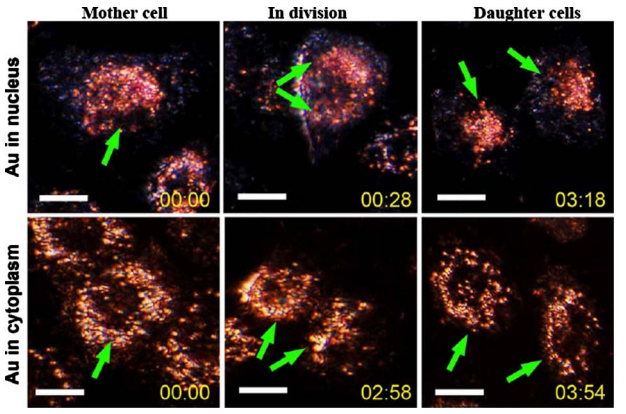

Fig. 5 Motion and distributon of Au NPs during cell mitosis. When the particles are localized in the nuclear region of mother cells, they remain in the nuclear region of daughter cells. When they are localized in the cytopalsm of mother cells, they remain in the cytoplasm of daughter cells (also see Video 3 and 4). The cells were incubated with 0.1 nM RGD/NLS/PEG (top) and RGD/PEG (bottom) conjugated Au NPs in cell culture medium at 37 °C overnight before the tracking experiment. Scale bar: 10 μm. The time is shown as hour:minute.

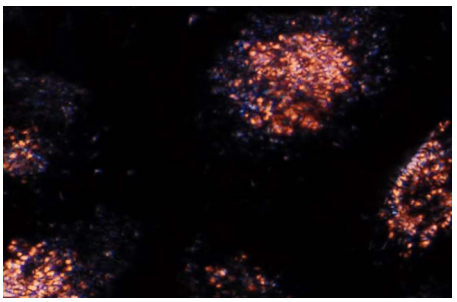

Video 3 Movement and distributon of Au NPs initially inside the nucleus during cell mitosis (QuickTime, 1.79 MB).
[URL: http://dx.doi.org/10.1117/1.3477179.3]

division. As explained previously, the preservation of Au NPs in the nuclear region is possibly due to the binding of the NPs to the chromosomes. The preservation in the cytoplasmic region is probably due to NP encapsulation in endosomes, which keep them inside the cytoplasm duiring mitosis.

3.5 *Visualizing the Effects of Au NPs on Cell Viability*

Another application of this imaging technique is the observation of the effects of Au NPs on the viability of daughter cells. In our experiments, we found that Au NPs did not induce any effect on the cell growth or division, nor on the growth of daughter cells until the dose of RGD/NLS/PEG-conjugated Au NPs added to the culture medium was increased above 0.4 nM. In the specific case shown in Fig. 6, we found that Au NPs were not equally divided between the two daughter cells, and the daughter cell with more Au NPs in the nucleus did not survive (see Video 5). Therefore, although Au NPs at a concentration of 0.4 nM do not have obvious effects on the parent cell (which remained alive until division), they could cause the death of the daughter cell in the later stages of cell division. This indicates the potential of developing Au NPs as anticancer drugs. Currently, we do not know much about the mechanism, but we have confirmed that the death of the daughter cell is a consequence of the DNA damage induced by the presence of the high density of Au NPs inside the cell nucleus.[55] Further investigation of the interaction between Au NPs and chromosomes will help us to develop Au NPs as drug for cancer therapy.

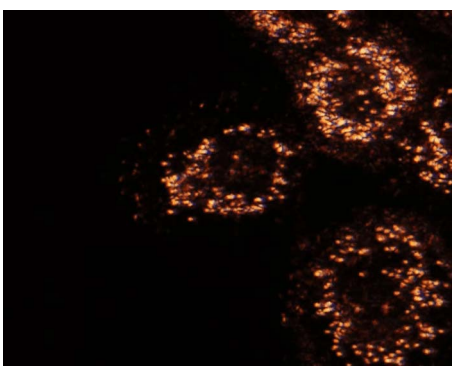

Video 4 Movement and distributon of Au NPs initially inside the cytoplasm during cell mitosis (QuickTime, 2.09 MB).
[URL: http://dx.doi.org/10.1117/1.3477179.4]

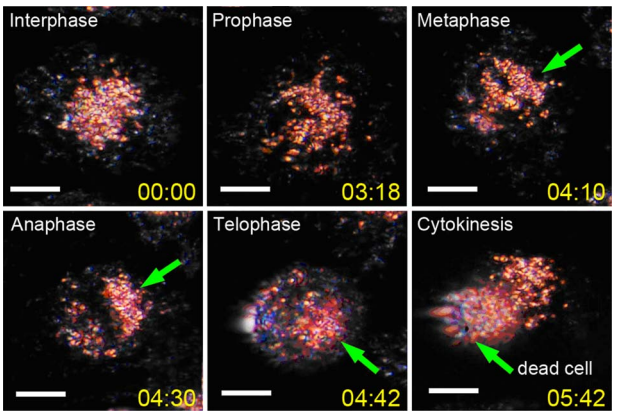

Fig. 6 Genotoxicity of high-dose Au NPs. In this case, the concentration of RGD/NLS/PEG-conjugated Au NPs is 0.4 nM. It is obvious that Au NPs are not equally divided among the two daughter cells and the daughter cell with more Au NPs in nucleus does not survive, as indicated by arrow (also see Video 5). The time is shown as hour:minute and the scale bar is 10 μm.

4 Conclusion

We showed the possibility of using plasmonic nanotechnology for live cell imaging and the study of various cellular processes that occurring inside the cytoplasm or, especially, the nuclear region over a long period of time (up to two cell cycles). The nuclear dynamics during cell mitosis was observed in real time in living cells. We showed that Au NPs inside the nuclear region could provide robust light scattering contrast agents to identify and study various stages of mitosis with the real-time dark-field light scattering imaging system we have developed. The final distribution of the Au NPs in the daughter cells depends on the initial location of the NPs in the parent cell. At the high concentration of 0.4 nM, while the NPs do not have an effect on parent cells, they induce death in the daughter cells. Dark-field imaging utilizing the enhanced light scattering signal from plasmonic NPs is a new emerging technology that extends and/or complements current mainstream fluorescence techniques. It is certain that further technological developments in this area will increase our understanding of cellular processes and functions and provide us with new strategies for disease diagnosis and therapy.

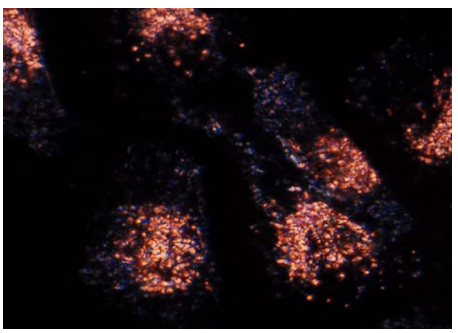

Video 5 Effects of bioconjugated Au NPs on the viability of daughter cells under a high dose (QuickTime, 1.5 MB).
[URL: http://dx.doi.org/10.1117/1.3477179.5]

Acknowledgments

We wish to thank the Department of Energy (Grant No. DE-FG02-97 ER 14799) for supporting this research. X. Huang would like to thank the distinguished CCNE postdoctoral fellowship at Emory-Georgia Tech Cancer Center for Nanotechnology Excellence. We thank Megan Mackey for her assistance in revising this manuscript.

References

1. W. Rudolph and M. Kempe, "Trends in optical biomedical imaging," *J. Mod. Opt.* **44**(9), 1617–1642 (1997).
2. C. Bremer, V. Ntziachristos, and R. Weissleder, "Optical-based molecular imaging: contrast agents and potential medical applications," *Eur. Radiol.* **13**(2), 231–243 (2003).
3. R. Parthasarathy and J. T. Groves, "Optical techniques for imaging membrane topography," *Cell Biochem. Biophys.* **41**(3), 391–414 (2004).
4. S. A. Boppart A. L. Oldenburg, C. Y. Xu, and D. L. Marks, "Optical probes and techniques for molecular contrast enhancement in coherence imaging," *J. Biomed. Opt.* **10**(4), 041208 (2005).
5. N. Thekkek and R. Richards-Kortum, "Optical imaging for cervical cancer detection: solutions for a continuing global problem," *Nat. Rev. Cancer* **8**(9), 725–731 (2008).
6. C. Balas, "Review of biomedical optical imaging—a powerful, non-invasive, non-ionizing technology for improving *in vivo* diagnosis," *Meas. Sci. Technol.* **20**, 104020 (2009).
7. G. Wang, A. S. Stender, W. Sun, and N. Fang, "Optical imaging of non-fluorescent nanoparticle probes in live cells," *Analyst* **135**(2), 215–221 (2010).
8. M. Dahan, S. Levi, C. Luccardini, P. Rostaing, B. Riveau, and A. Triller, "Diffusion dynamics of glycine receptors revealed by single-quantum dot tracking," *Science* **302**(5644), 442–445 (2003).
9. J. K. Jaiswal, H. Mattoussi, J. M. Mauro, and S. M. Simon, "Long-term multiple color imaging of live cells using quantum dot bioconjugates," *Nat. Biotechnol.* **21**(1), 47–51 (2003).
10. C. J. Weijer, "Visualizing signals moving in cells," *Science* **300**(5616), 96–100 (2003).
11. X. Michalet, F. F. Pinaud, L. A. Bentolila, J. M. Tsay, S. Doose, J. J. Li, G. Sundaresan, A. M. Wu, S. S. Gambhir, and S. Weiss, "Quantum dots for live cells, *in vivo* imaging, and diagnostics," *Science* **307**(5709), 538–544 (2005).
12. K. I. Willig, S. O. Rizzoli, V. Westphal, R. Jahn, and S. W. Hell, "STED microscopy reveals that synaptotagmin remains clustered after synaptic vesicle exocytosis," *Nature* **440**(7086), 935–939 (2006).
13. B. Huang, W. Q. Wang, M. Bates, and X. W. Zhuang, "Three-dimensional superresolution imaging by stochastic optical reconstruction microscopy," *Science* **319**(5864), 810–813 (2008).
14. M. J. Kallio, V. A. Beardmore, J. Weinstein, and G. J. Gorbsky, "Rapid microtubule-independent dynamics of Cdc20 at kinetochores and centrosomes in mammalian cells," *J. Cell Biol.* **158**(5), 841–847 (2002).
15. G. H. Patterson and J. Lippincott-Schwartz, "A photoactivatable GFP for selective photolabeling of proteins and cells," *Science* **297**(5588), 1873–1877 (2002).
16. P. Kalab, K. Weis, and R. Heald, "Visualization of a Ran-GTP gradient in interphase and mitotic Xenopus egg extracts," *Science* **295**(5564), 2452–2456 (2002).
17. J. Lippincott-Schwartz and G. H. Patterson, "Development and use of fluorescent protein markers in living cells," *Science* **300**(5616), 87–91 (2003).
18. M. J. Saxton and K. Jacobson, "Single-particle tracking: applications to membrane dynamics," *Annu. Rev. Biophys. Biomol. Struct.* **26**, 373–399 (1997).
19. B. Schuler, E. A. Lipman, and W. A. Eaton, "Probing the free-energy surface for protein folding with single-molecule fluorescence spectroscopy," *Nature* **419**(6908), 743–747 (2002).
20. Y. Ohsugi, K. Saito, M. Tamura, and M. Kinjo, "Lateral mobility of membrane-binding proteins in living cells measured by total internal reflection fluorescence correlation spectroscopy," *Biophys. J.* **91**(9), 3456–3464 (2006).
21. H. P. Babcock, C. Chen, and X. W. Zhuang, "Using single-particle tracking to study nuclear trafficking of viral genes," *Biophys. J.* **87**(4), 2749–2758 (2004).
22. B. Brandenburg and X. W. Zhuang, "Virus trafficking—learning from single-virus tracking," *Nat. Rev. Microbiol.* **5**(3), 197–208 (2007).
23. C. H. Foyer, P. Descourvieres, and K. J. Kunert, "Protection against oxygen radicals—an important defense-mechanism studied in transgenic plants," *Plant, Cell Environ.* **17**(5), 507–523 (1994).
24. L. L. Song, C. A. G. O. Varma, J. W. Verhoeven, and H. J. Tanke, "Influence of the triplet excited state on the photobleaching kinetics of fluorescein in microscopy," *Biophys. J.* **70**(6), 2959–2968 (1996).
25. M. Soszynski and G. Bartosz, "Decrease in accessible thiols as an index of oxidative damage to membrane proteins," *Free Radic Biol. Med.* **23**(3), 463–469 (1997).
26. L. L. Song, R. P. M. van Gijlswijk, I. T. Young, and H. J. Tanke, "Influence of fluorochrome labeling density on the photobleaching kinetics of fluorescein in microscopy," *Cytometry* **27**(3), 213–223 (1997).
27. A. Wright, W. A. Bubb, C. L. Hawkins, and M. J. Davies, "Singlet oxygen-mediated protein oxidation: Evidence for the formation of reactive side chain peroxides on tyrosine residues," *Photochem. Photobiol.* **76**(1), 35–46 (2002).
28. T. Bernas, M. Zarebski, P. R. Cook, and J. W. Dobrucki, "Minimizing photobleaching during confocal microscopy of fluorescent probes bound to chromatin: role of anoxia and photon flux," *J. Micros. Oxford* **215**, 281–295 (2004).
29. J. Yguerabide and E. E. Yguerabide, "Light-scattering submicroscopic particles as highly fluorescent analogs and their use as tracer labels in clinical and biological applications. I. Theory," *Anal. Biochem.* **262**(2), 137–156 (1998).
30. J. Yguerabide and E. E. Yguerabide, "Light-scattering submicroscopic particles as highly fluorescent analogs and their use as tracer labels in clinical and biological applications. II. Experimental characterization," *Anal. Biochem.* **262**(2), 157–186 (1998).
31. J. Yguerabide and E. E. Yguerabide, "Resonance light scattering particles as ultrasensitive labels for detection of analytes in a wide range of applications," *J. Cell Biochem. Suppl.* **37**(S37, Suppl.), 71–81 (2001).
32. K. Sokolov, M. Follen, J. Aaron, I. Pavlova, A. Malpica, R. Lotan, and R. Richartz-Kortum, "Real-time vital optical imaging of precancer using anti-epidermal growth factor receptor antibodies conjugated to gold nanoparticles," *Cancer Res.* **63**(9), 1999–2004 (2003).
33. I. H. El-Sayed, X. Huang, and M. A. El-Sayed, "Surface plasmon resonance scattering and absorption of anti-EGFR antibody conjugated gold nanoparticles in cancer diagnostics: applications in oral cancer," *Nano Lett.* **5**(5), 829–834 (2005).
34. J. Aaron, N. Nitin, K. Travis, S. Kumar, T. Collier, S. Y. Park, M. Jose-Yacaman, L. Coghlan, M. Follen, R. Richards-Kortum, and K. Sokolov, "Plasmon resonance coupling of metal nanoparticles for molecular imaging of carcinogenesis *in vivo*," *J. Biomed. Opt.* **12**(3), 034007 (2007).
35. J. W. Stone, P. N. Sisco, E. C. Goldsmith, S. C. Baxter, and C. J. Murphy, "Using gold nanorods to probe cell-induced collagen deformation," *Nano Lett.* **7**(1), 116–119 (2007).
36. C. J. Murphy, A. M. Gole, J. W. Stone, P. N. Sisco, A. M. Alkilany, E. C. Goldsmith, and S. C. Baxter, "Gold nanoparticles in biology: beyond toxicity to cellular imaging," *Acc. Chem. Res.* **41**(12), 1721–1730 (2008).
37. Y. Hu, Q. Chen, Y. Ding, R. T. Li, X. Q. Jiang, and B. R. Liu, "Entering and Lighting Up Nuclei Using Hollow Chitosan-Gold Hybrid Nanospheres," *Adv. Mater.* **21**(36), 3639–3643 (2009).
38. S. Kumar, N. Harrison, R. Richards-Kortum, and K. Sokolov, "Plasmonic nanosensors for imaging intracellular biomarkers in live cells," *Nano Lett.* **7**(5), 1338–1343 (2007).
39. G. X. Rong, H. Y. Wang, L. R. Skewis, and B. M. Reinhard, "Resolving sub-diffraction limit encounters in nanoparticle tracking using live cell plasmon coupling microscopy," *Nano Lett.* **8**(10), 3386–3393 (2008).
40. J. Aaron, K. Travis, N. Harrison, and K. Sokolov, "Dynamic imaging of molecular assemblies in live cells based on nanoparticle plasmon resonance coupling," *Nano Lett.* **9**(10), 3612–3618 (2009).
41. Y. W. Jun, S. Sheikholeslami, D. R. Hostetter, C. Tajon, C. S. Craik, and A. P. Alivisatos, "Continuous imaging of plasmon rulers in live cells reveals early-stage caspase-3 activation at the single-molecule level," *Proc. Natl. Acad. Sci. U.S.A.* **106**(42), 17735–17740 (2009).

42. J. Turkevich, P. C. Stvenson, and J. Hillier, "A study of the nucleation and growth processes in the synthesis of colloidal gold," *Discuss. Faraday Soc.* **11**, 55–75 (1951).
43. G. Frens, "Controlled nucleation for the regulation of the particle size in monodisperse gold suspensions," *Nature (London), Phys. Sci.* **241**(105), 20–22 (1973).
44. S. J. Hurst, A. K. R. Lytton-Jean, and C. A. Mirkin, "Maximizing DNA loading on a range of gold nanoparticle sizes," *Anal. Chem.* **78**(24), 8313–8318 (2006).
45. A. G. Tkachenko, H. Xie, D. Coleman, W. Glomm, J. Ryan, M. F. Anderson, S. Franzen, and D. L. Feldheim, "Multifunctional gold nanoparticle-peptide complexes for nuclear targeting," *J. Am. Chem. Soc.* **125**(16), 4700–4701 (2003).
46. A. G. Tkachenko, H. Xie, Y. Liu, D. Coleman, J. Ryan, W. R. Glomm, M. K. Shipton, S. Franzen, and D. L. Feldheim, "Cellular trajectories of peptide-modified gold particle complexes: comparison of nuclear localization signals and peptide transduction domains," *Bioconjugate Chem.* **15**(3), 482–490 (2004).
47. A. K. Oyelere, B. Chen, X. Huang, I. H. El-Sayed, and M. A. El-Sayed, "Peptide conjugated gold nanorods for nuclear targeting," *Bioconjugate Chem.* **18**(5), 1490–1497 (2007).
48. S. Nakielny and G. Dreyfuss, "Transport of proteins and RNAs in and out of the nucleus," *Cell* **99**(7), 677–690 (1999).
49. V. Escriou, M. Carrie're, D. Scherman, and P. Wils, "N LS bioconjugates for targeting therapeutic genes to the nucleus," *Adv. Drug Delivery Rev.* **55**, 295–306 (2003).
50. W. Xie, L. Wang, Y. Zhang, L. Su, A. Shen, J. Tan, and J. Hu, "Nuclear targeted nanoprobe for single living cell detection by surface-enhanced raman scattering," *Bioconjugate Chem.* **20**(4), 768–773 (2009).
51. J. A. Ryan, K. W. Overton, M. E. Speight, C. N. Oldenburg, L. Loo, W. Robarge, S. Franzen, and D. L. Feldheim, "Cellular uptake of gold nanoparticles passivated with BSA-SV40 large T antigen conjugates," *Anal. Chem.* **79**(23), 9150–9159 (2007).
52. W. Cai, D. M. Shin, K. Chen, O. Gheysens, Q. Cao, S. X. Wang, S. S. Gambhir, and X. Chen, "Peptide-labeled near-infrared quantum dots for imaging tumor vasculature in living subjects," *Nano Lett.* **6**(4), 669–676 (2006).
53. W. Cai and X. Chen, "Preparation of peptide-conjugated quantum dots for tumor vasculature-targeted imaging," *Nat. Protoc.* **3**, 89–96 (2008).
54. Z. Li, P. Huang, X. Zhang, J. Lin, S. Yang, B. Liu, F. Gao, P. Xi, Q. Ren, and D. Cui, "RGD-conjugated dendrimer-modified gold nanorods for *in vivo* tumor targeting and photothermal therapy," *Molec. Pharmaceut.* **7**(1), 94–104 (2010).
55. B. Kang, M. Mackey, and M. A. El-Sayed, "Nuclear targeting of gold nanoparticles in cancer cells induces DNA damage, causing cytokinesis arrest and apoptosis," *J. Am. Chem. Soc.* **132**(5), 1517–1518 (2010).
56. P. K. Jain, W. Huang, and M. A. El-Sayed, "On the universal scaling behavior of the distance decay of plasmon coupling in metal nanoparticle pairs: a plasmon ruler equation," *Nano Lett.* **7**(7), 2080–2088 (2007).
57. P. K. Jain and M. A. El-Sayed, "Surface plasmon coupling and its universal size scaling in metal nanostructures of complex geometry: elongated particle pairs and nanosphere trimers," *J. Phys. Chem. C* **112**(13), 4954–4960 (2008).
58. C. Tabor, R. Murali, M. A. Mahmoud, and M. A. El-Sayed "On the use of plasmonic nanoparticle pairs as a plasmon ruler: the dependence of the near-field dipole plasmon coupling on nanoparticle size and shape," *J. Phys. Chem. A* **113**(10), 1946–1953 (2009).
59. G. Ostergren, J. Molebajer, and A. Bajer, "An Interpretation of Transport Phenomena at Mitosis," *Ann. N.Y. Acad. Sci.* **90**(2), 381–408 (1960).
60. S. Inoue and H. Sato, "Cell motility by labile association of molecules—nature of mitotic spindle fibers and their role in chromosome movement," *Gen. Physiol.* **50**(6), 259–292 (1967).
61. S. Inoue, "Video image-processing greatly enhances contrast, quality, and speed in polarization-based microscopy," *J. Cell Biol.* **89**(2), 346–356 (1981).